Optimization of Tape Casting for Fabrication of $Li_{6.25}Al_{0.25}La_3Zr_2O_{12}$ Sheets

*Robert A. Jonson, Eongyu Yi, Fengyu Shen, Michael C. Tucker**

Lawrence Berkeley National Laboratory, 1 Cyclotron Road, Berkeley CA 94720, USA

Solid state battery, lithium garnet, LLZO, tape casting, sintering

TABLE OF CONTENTS GRAPHIC

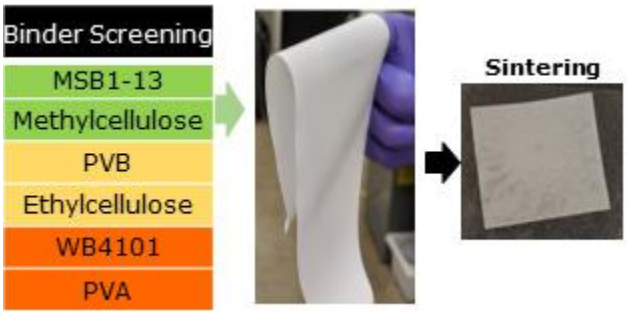

ABSTRACT

Tape casting is an attractive technology for the scalable manufacturing of thin lithium garnet electrolyte (LLZO) layers for solid state battery applications. Processing of LLZO is complicated by many factors including lithium volatilization, abnormal grain growth and phase instability which are exacerbated by high surface area to volume ratios. In this work a sintering protocol for commercially available $Li_{6.25}Al_{0.25}La_3Zr_2O_{12}$ (Al-LLZO) powder was developed that requires no

mother-powder covering or externally applied pressure. MgO was investigated as a sintering additive to improve density and ionic conductivity of the Al-LLZO sheets and produce a fine-grained microstructure. Al-LLZO sheets with 5 wt% MgO had densities of >90 % and ionic conductivity >$2x10^{-4}$ S/cm. The optimized ceramic composition and sintering protocol were used to compare several tape casting binder systems. A "green" water-based system using methylcellulose as a binder was developed with green and final properties comparable to those obtained with solvent-based systems.

INTRODUCTION

The lithium-garnet electrolyte, nominally $Li_7La_3Zr_2O_{12}$ (LLZO), has attracted considerable attention as an electrolyte material for safer next-generation solid-state lithium batteries owing to its combination of high ionic conductivity (up to 10^{-3} S/cm at room temperature, depending on dopants [1, 2]), apparent stability against metallic lithium [3], and wide electrochemical stability window [4, 5]. While LLZO's properties are appealing, it is a difficult material to process with scalable techniques, e.g. tape casting, particularly because of the challenge of sintering LLZO ceramics to high density while controlling Li content.

The high bulk ionic conductivity of LLZO is dependent on obtaining the cubic polymorph of the material rather than the tetragonal phase, for which ionic conductivity is over two orders of magnitude lower [6]. The cubic phase is typically stabilized through aliovalent substitution with the most common being Al or Ga for Li, or Ta or Nb for Zr [1, 2, 7, 8]. These stabilize the cubic phase and improve conductivity *via* creation of vacancies and disorder in lithium-site populations [6, 9, 10].

Controlling lithium content in LLZO can be seen as critical for obtaining high performance electrolytes. Control of the Li content is, however, complicated by lithium evaporation from LLZO at the 1000 to 1250°C sintering temperature required to achieve high density. Because of Li evaporation, non-conductive impurity phases such as $La_2Zr_2O_7$ are easily formed. Common strategies to mitigate Li loss involve adding excess Li, often in the form of Li_2CO_3, and/or burying samples in sacrificial mother LLZO powder [11, 12]. Since covering with sacrificial mother powder is not expected to be a viable solution at manufacturing scale, other options must be investigated. Addition of excess lithium to the green part requires an optimization of sintering temperature and time, and Li_2CO_3 content that depends on sample volume and surface area, among other considerations [13, 14]. This means that optimization done with pelletized samples will not apply directly to thin tape cast sheets. Furthermore, even when cubic LLZO is obtained, it is sensitive to a surplus of Li [12]. For example, Ga-LLZO suffers a 20% drop in conductivity from a peak of $1.1x10^{-3}$ S/cm as lithium concentration increases from 6.55 to 6.79 per formula unit [15].

Reducing sintering temperature and/or time may also reduce the required excess lithium content. Sintering aids have been identified for LLZO, with various mechanisms of densification enhancement. Al_2O_3 forms a eutectic liquid phase with LiO_2 at 1055°C, which promotes particle rearrangement and aids in diffusion [12, 16]. MgO inhibits grain growth, resulting in higher density and more uniform microstructure [17, 18]. Huang et al. [19] reported that adding >5 wt% MgO to Ta-substituted LLZO controlled abnormal grain growth (AGG); increased fracture strength by 50%; and achieved high density comparable to hot pressing (98%). However, conductivity was reduced moderately from 6.7 to $5.8x10^{-4}$ S/cm. In this study, we elucidate the role of slurry formulation and sintering additives on the fabrication of dense, thin tape cast LLZO sheets. The

impact of sample geometry on the optimization of Li content, sintering additives, and sintering protocol is demonstrated for the cases of thick pellets and thin tape cast sheets.

Tape casting is one of the most widely used methods for producing thin ceramic sheets in a continuous process. A typical tape casting process proceeds in several stages [20]. First, ceramic powder is ball milled in a solvent containing a dispersant to break apart agglomerates and produce a stable suspension. Next, binder and plasticizers are added and mixed for a period of time. Finally, the slurry is cast with a doctor blade onto a carrier sheet to produce a tape with uniform height. Selection of the solvent, dispersant, binder, other additives, and their ratios depends on the physical and chemical properties of the ceramic power to be cast and the desired properties of the green tape.

Tape casting of LLZO sheets and bi- and tri-layer structures is common, and Table 1 presents several examples. Popular slurry components are Menhaden fish oil dispersant, polyvinyl butyral binder, and either an ethanol- or toluene-based solvent mixture [13, 14, 21-26]. Ye et al. report an aqueous system using methylcellulose as a binder with polyethylene glycol and glycerol as plasticizers [27]. Other aqueous slurries have been used for preparing porous structures via freeze casting [26-28]. Unfortunately, the details of tape slurry optimization, selection of slurry components, and green density of tapes are generally not reported. Direct comparison of these tape casting binder/solvent systems is complicated by the wide range of ceramic composition and variation in powder properties such as particle size distribution and surface area used in previous studies.

Table 1. Examples of LLZO Tape Casting

Solvent	Dispersant	Binder	Plasticizer	Ceramic	Density (%)	Conductivity (S/cm x10^{-4})	Ref.

Ethanol, Butyl Acetate		Polyacrylic resin	Methyl benzoate	Ta-LLZO, Li2O	99	5.2	[29]
Ethanol	Menhaden fish oil	PVB	Benzyl butyl phthalate, polyethylene glycol	Al-LLZO, ZnO		.8	[21]
Ethanol, Toluene	"	"	"	"			
Ethanol, Xylene	"	"	"	"			
Ethanol, Acetone	Polyacrylic acid (Mn 2000)	PVB	Benzyl butyl phthalate	Al-LLZO	94	2.0	[13, 14, 26]
Ethanol, Toluene	Menhaden fish oil	Ethyl-cellulose	Dibutyl phthalate, polyethylene glycol	Nb, Al-LLZO, Li3BO3	90.8	2.8	[30]
Ethylene glycol monoethyl ether		PVB	Glycerol trioleate	Ta-LLZO	Porous bilayer		[31]
Toluene, Isopropanol	Fish oil	PVB	benzyl butyl phthalate	Ca, Nb-LLZO	Porous bilayer	2.2	[22, 23]
Toluene, Isopropanol	Menhaden fish oil	PVB	polyalkylene glycol	Ca, Nb-LLZO	Porous bilayer	5.35 for dense layer	[24]
Water	Ammonium polymeth-acrylate	Acrylic emulsion, xanthan gum		Al-LLZO	~95	5.0	[26, 28]
Ethanol, Butanone	Castor oil	PVB	Dibutyl phthalate	Al-LLZO		.34	[25]
Water		Methyl-cellulose	Polyethylene glycol, glycerol	Al, Ta-LLZO	~90	1.5	[27]
Water, Ethanol	Dispex Ultra PA 4560	Methyl-cellulose	Polyethylene glycol	Al-LLZO, MgO	91.1	2.3	This Work
Toluene, Xylenes	DS002	MSB1-13		Al-LLZO, MgO	87.9	1.7	This Work

To overcome these limitations of the previous efforts, a detailed examination of the tape casting process as it pertains to Al-LLZO is provided here. Several tape casting slurry systems are screened, and selected candidate systems are optimized to produce high green oxide-only density (GOOD). The impact of this optimization on mechanical properties of the green tape and final density of the sintered Al-LLZO sheet is also examined. In order to enhance reproducibility and isolate the processing and additive variables, a single lot of commercially-available Al-doped LLZO is used throughout.

EXPERIMENTAL

Tape Preparation

Dispersant content in the tape casting slurries was screened and optimized through settling experiments [20]. Al-LLZO powder ($Li_{6.25}Al_{0.25}La_3Zr_2O_{12}$, 500 nm, MSE Supplies) with MgO (50 nm, US Research Nanomaterials Inc.) and Li_2CO_3 (Alfa Aesar) were ball milled together with solvent and the corresponding dispersants shown in Table 2. ZrO_2 balls with a 2mm diameter (Inframat) were used as milling media. A 5mL portion of each slurry was pipetted into a graduated test tube and sealed. The dispersions were allowed to settle for 2 weeks. Shorter, and thus denser, packed bed height after settling indicates better quality of dispersion.

Table 2. Solvents and Dispersants Screened for Tape Casting

Solvent	Dispersant Candidates
Toluene	Menhaden Fish Oil (Tape Casting Warehouse) DS002 (Polymer Innovations)
75/25 Water/Ethanol	Poly(acrylic acid) Dispex Ultra PA 4560 (BASF) Hypermer KD6 (Croda International)

	Hypermer KD7 (Croda)

All tape slurries were mixed in a two stage process. In the first stage the Al-LLZO, Li_2CO_3 and MgO were milled overnight with the corresponding solvent, dispersant, and other additives using ZrO_2 media to produce a ceramic dispersion. All tapes contained 5 wt% of additional Li_2CO_3 which corresponds to 19.2 wt% excess Li. In the second stage the binder and plasticizers were added to the mixture and milled overnight again. Table 3 lists the binder systems and their specific additives. Detailed slurry compositions can be found in Table S1 in the supplemental information.

Table 3. Binder Systems Screened for Tape Casting of Al-LLZO

Binder	**Solvent**	**Dispersant**	**Plasticizer**	**Additional**
Poly(vinyl alcohol)	Water	Dispex		DF002 Defoamer (Polymer Innovations)
WB4101 (Polymer Innovations)	Water	-	-	DF002 Defoamer
Ethylcellulose	75% Toluene 25% Water	DS002	Polyethylene Glycol 300 (PEG 300, Sigma Aldrich)	DF002 Defoamer
Poly(vinyl butyral)	50% Ethanol 50% Toluene	-	Benzyl butyl phthalate	
MSB 1-13 (Polymer Innovations)	Toluene	DS002		
Methylcellulose (25cp, Alfa Aesar)	75%wt. Water 25%wt. Ethanol	Dispex	PEG 300	DF002 Defoamer Dynol 604 Wetting Agent (Evonik Industries)

Following mixing, the slurries were de-aired under vacuum for 10 minutes. Tapes were cast onto a silicone-coated polyethylene terephthalate (SiPET) carrier film with an automatic doctor blade coater (MTI Corporation). The doctor blade gap was set to 200µm. Films were dried overnight at ambient conditions. Tapes were removed from the carrier film and cut into squares approximately 4.5 cm in width. Four squares were stacked between SiPET sheets and laminated together at pressures ranging from 10 to 35 MPa and temperatures between 100 and 150°C for 15 minutes. These laminates were then subdivided into squares approximately 2 cm in width. The tape laminate sheets were then debinded at 700°C in air for 2 h with a ramp rate of 2°C/min. Laminate sheets were sintered between pyrolytic graphite sheets (Panasonic) in order to prevent interactions with the top and bottom Al_2O_3 setter plates used to mitigate warping. Sintering was performed in a tube furnace (MTI) under a flowing Ar atmosphere at 1115°C for a range of times between 2 and 5 h. The inert Ar atmosphere prevents both the oxidation of the graphite sheets and the formation of Li_2CO_3 on the Al-LLZO part during cooling[32]. Sintering temperature was selected on the basis of dilatometry data which indicated an onset of sintering for MgO-containing Al-LLZO at approximately 1115°C (Figure S1).

Pellet Preparation

Al-LLZO pellet samples with 0, 3, 5 and 7 wt%. MgO and 3 wt.%. Li_2CO_3 were made as a low-surface-area specimen geometry for comparison with the tape samples. The Li_2CO_3 content was reduced to 3%wt. in order to compensate for the greatly reduced surface area of the pellets when compared to the tape laminates. The Al-LLZO, MgO and Li_2CO_3 were milled overnight in isopropyl alcohol with ZrO_2 media. The powder was dried and pressed in a ¼" pellet die at 400 MPa. The pellets were sintered in a tube furnace for 7 h at 1115°C under flowing argon using pyrolytic graphite sheets as substrates.

Characterization

A bending test was used for semi-quantitative characterization of green tape mechanical properties. A section of green tape was bent around a series of rods with successively smaller diameter ranging from 14mm to 2mm. The lowest radius that a tape could be bent around without breaking was recorded. Slurry viscosity was measured on a Brookfield DV-II+ Pro cone-and-plate viscometer with a 1.5° cone angle (Table S2). Ionic conductivity was measured by electronic impedance spectroscopy using a Biologic VSP-300 potentiostat. Electrical contacts on tape laminate samples were made by sputtering 4mm diameter gold contact pads on opposing sides with an aligned mask. Pellet samples were polished flat with 600 grit paper before gold was sputtered onto their flat surfaces. Frequency was swept from 7 MHz to 10 Hz with an amplitude of 10 mV. Phase analysis was performed on crushed samples by XRD with a Bruker D2 system using Cu α radiation. Rietveld refinement was carried out on the XRD patterns with the FullProf package using the Match! 3 program (Crystal Impact GbR). Scanning electron microscopy (SEM) imaging was performed with a JEOL JSM-6500F microscope in secondary electron mode. SEM samples were prepared by sputtering gold on a fresh facture surface of either a tape laminate or pellet.

RESULTS AND DISCUSSION

Optimization of Sintering Conditions

The Al-LLZO sintering process is sensitive to Li volatilization and sintering additives. To determine the effects of tape casting binder systems on the final properties of Al-LLZO sheets it is important to have an optimized sintering protocol and ceramic composition. The following section describes the optimization of sintering conditions and MgO sintering additive content for the sample geometry used for the binder system comparison.

Sintering Tape Cast Sheets

Optimization of MgO content and sintering time for Al-LLZO laminate sheets was performed by examining the density and ionic conductivity of sheets sintered with a range of MgO contents between 0 and 7 wt%. at 1115°C for 2 to 5 h (Figure 1). All of the sheets contained 5 wt%. Li_2CO_3 for mitigation of Li evaporation. These tape laminates were made with the methylcellulose binder system, the specifics of which will be discussed in a later section. Sintered sheets were approximately 1.5cm on edge and 100µm thick for a surface area to volume ratio of approximately 150 cm^{-1}. Table 4 provides a summary of the sintered tape properties.

Table 4: Summary of Tape Sintering Optimization

Sintering Time (h.)	MgO (Wt%)	Average Ionic Conductivity (S/cm x10-4)	Average Density (%)	Phase	Lattice Parameter (Å)
2	0	-	84.1±0.8	Tetragonal	-
	3	0.45±0.04	90±2	Tetragonal	-
	5	1±0.1	88±4	Tetragonal	-
	7	0.6±0.2	87±5	Tetragonal	-
3	0	2.9±0.2	89.3±0.4	Cubic	12.967
	3	4.2±0.9	87.8±0.9	Cubic	12.968
	5	2.3±0.4	91.0±0.8	Cubic	12.968
	7	0.3±0.1	91±5	Cubic	12.967
4	0	2.28±0.01	90.9±0.2	Cubic	12.965
	3	2.8±0.8	88±2	Cubic	12.966
	5	0.41±0.2	90±4	Cubic	12.965

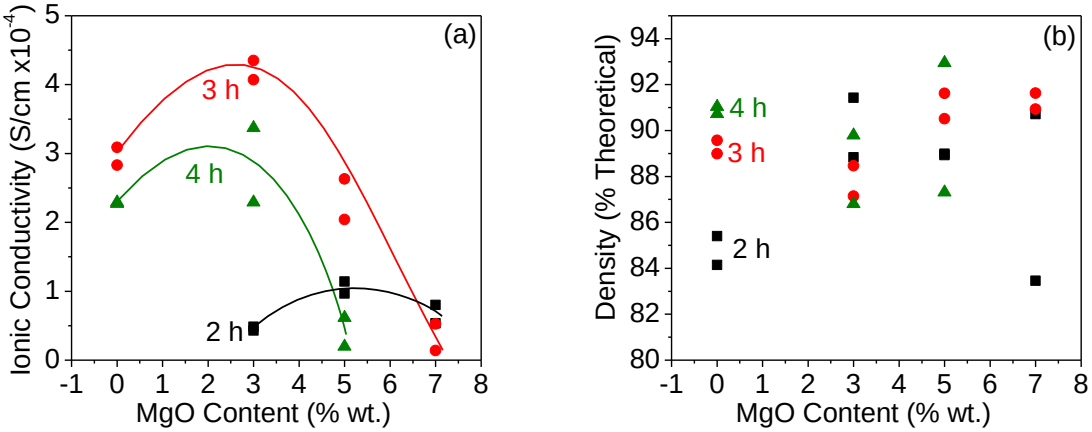

Figure 1. Optimization of sintering additives and sintering time for ~100 µm thick Al-LLZO sheets with 5 wt%. Li_2CO_3. (a) Ionic conductivity and (b) density for Al-LLZO sheets with a range of MgO content sintered at 1115°C for 2 (black), 3 (red) and 4 h (green). The lines are a guide for the eye.

Ionic conductivity reaches a maximum of 4.35×10^{-4} S/cm for sheets with 3 wt%. MgO sintered for 3 h, an increase of nearly 50% from sheets without any MgO at the same sintering conditions. Increasing MgO content beyond 3 wt% at 3 h of sintering time reduced conductivity; the 7 wt%. MgO sheets display less than 1×10^{-4} S/cm. Ionic conductivity was reduced for all samples with 4 h of sintering compared to 3 h but a similar trend in conductivity was observed, with 3 wt% MgO having the highest conductivity and additional MgO being detrimental.

Sintering for 2 h produced $<1 \times 10^{-4}$ S/cm conductivity in all MgO contents. Ionic conductivity and density were not strongly correlated. Densities of sheets sintered without MgO increased with longer sintering times, improving from ~85% with 2 h sintering to 91% at 4 h. Density for sheets containing MgO did not follow this trend and was highly variable. At 3 h of sintering time 5 and 7 wt% MgO improved density over 0 wt% MgO by 3 percentage points to ~91%. The 3 wt%. MgO sheets sintered for 3 h, which displayed the highest conductivity, were less dense than the others

by 1-4 percentage points. These trends suggest an engineering trade-off may be required between ionic conductivity and density.

Phase analysis provides further insight into the density and conductivity trends **Figure 2**(Figure 2). As described above, all of the samples sintered for 2 h, regardless of MgO content, demonstrated poor ionic conductivity. This is because these sheets contain the low ionic conductivity tetragonal LLZO phase, indicated by XRD peak splitting. The tetragonal phase arises from excess Li present in the garnet structure after sintering. Longer sintering times are expected to enhance Li evaporation and thereby promote transition to the cubic phase. Indeed, all samples sintered for 3 h or longer are cubic. Excess Li loss also reduces conductivity. The presence of $La_2Zr_2O_7$ is an indicator of Li deficiency and this may partially explain the reduced conductivity of the 4 h sintered samples, even though their density is within the same range as the 3 h samples. A low-intensity $La_2Zr_2O_7$ peak is observed at 28.5° in the 4 h sintered sheet with 0 wt%. MgO. This small peak is not visible in any of the samples containing MgO at either 4 or 5h. Unidentified impurity peaks are observed at 31.3° and 31.6° in the case of high MgO content (7 wt%) sheets sintered for 3 and 5 h. This suggests that MgO is not chemically inert, and interacts with Al-LLZO, which may account for the reduced ionic conductivity of the 5 and 7 wt% MgO sheets and the lack of $La_2Zr_2O_7$ in these samples at longer sintering times. The lattice parameters calculated for the sheets (Table 4) change little over the range of MgO content which does not provide conclusive evidence to whether Mg is or is not being doped into the LLZO.

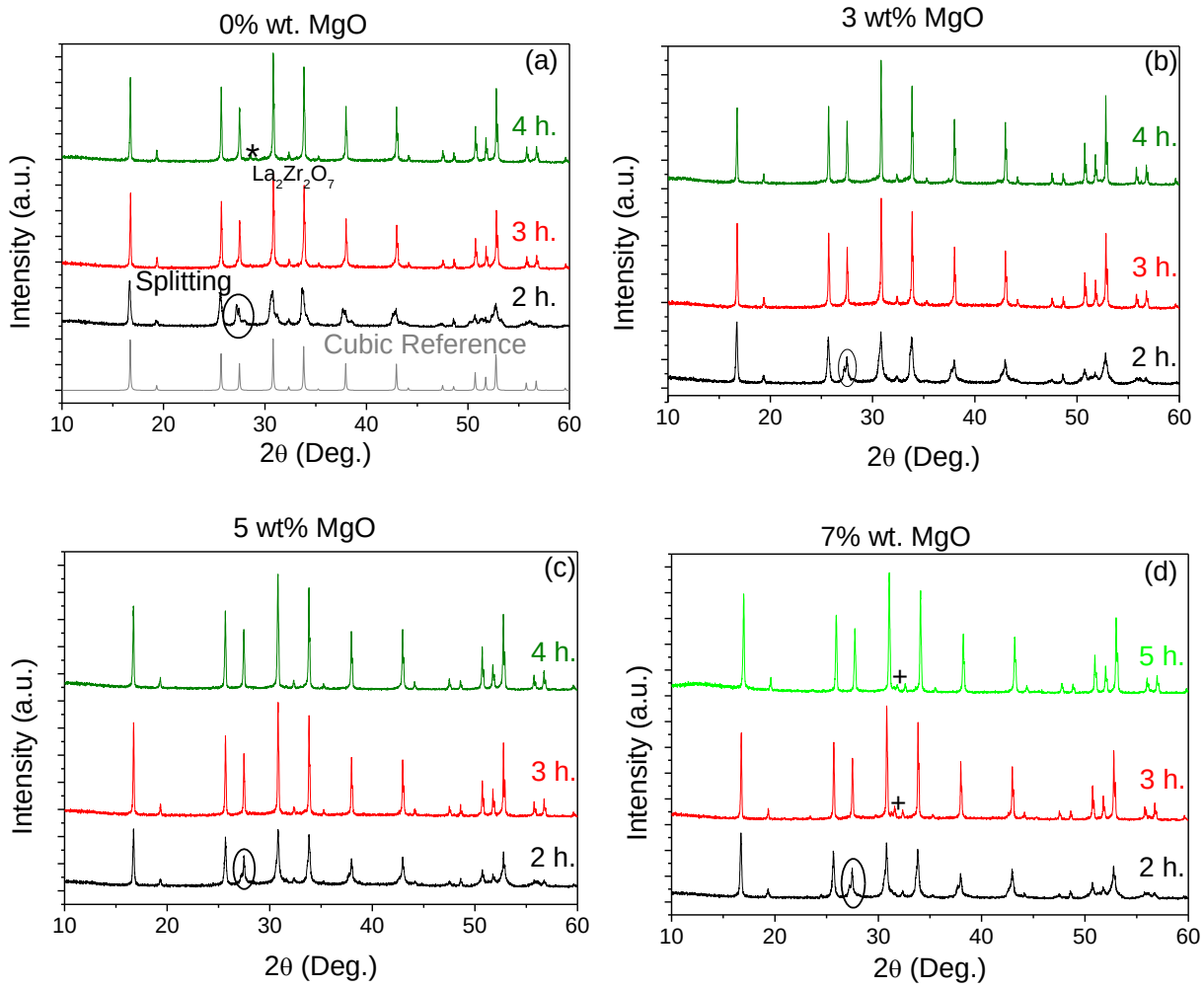

Figure 2. Phase analysis of selected ~100 µm thick Al-LLZO sheets. XRD patterns of Al-LLZO sheets sintered at 2 (black), 3 (red), and 4 (green) h with (a) 0 wt%. MgO, (b) 3 wt% MgO, (c) 5 wt% MgO, and (d) 7 wt%, MgO sintered at 2, 3, and 5 (green) h. A reference pattern for cubic LLZO is provided (grey, a). $La_2Zr_2O_7$ is identified by a *. Peak splitting from tetragonal LLZO is circled. The unidentified impurity peaks are marked by a +. The peak shift present in the 5 h sintered 7 wt%. MgO sample is an artifact produced by a sample holder that was at a different height.

Finer-grained structures are expected to be advantageous for battery applications because of its increased toughness, and are promoted by addition of MgO. SEM imaging (Figure 3) displays the

microstructural effects of adding MgO to the Al-LLZO sheets. The Al-LLZO sheets with 0 wt%. MgO did not have discernable grain boundaries but did contain large (>2μm) intragranular pores which are indicative of AGG. Addition of at least 3 wt%. MgO inhibited grain growth and produced reduced grain size (<5μm) and smaller pores (<1μm) concentrated at the grain boundaries. Additional MgO (5 wt%) did not appear to further impact microstructure at these conditions.

Based on these observations, 5 wt% MgO and 5 wt% Li_2CO_3 sintered for 3 h were used for evaluation of the tape casting process, described below, because it had the highest density in addition to a fine-grained microstructure and ionic conductivity >$2x10^{-4}$ S/cm.

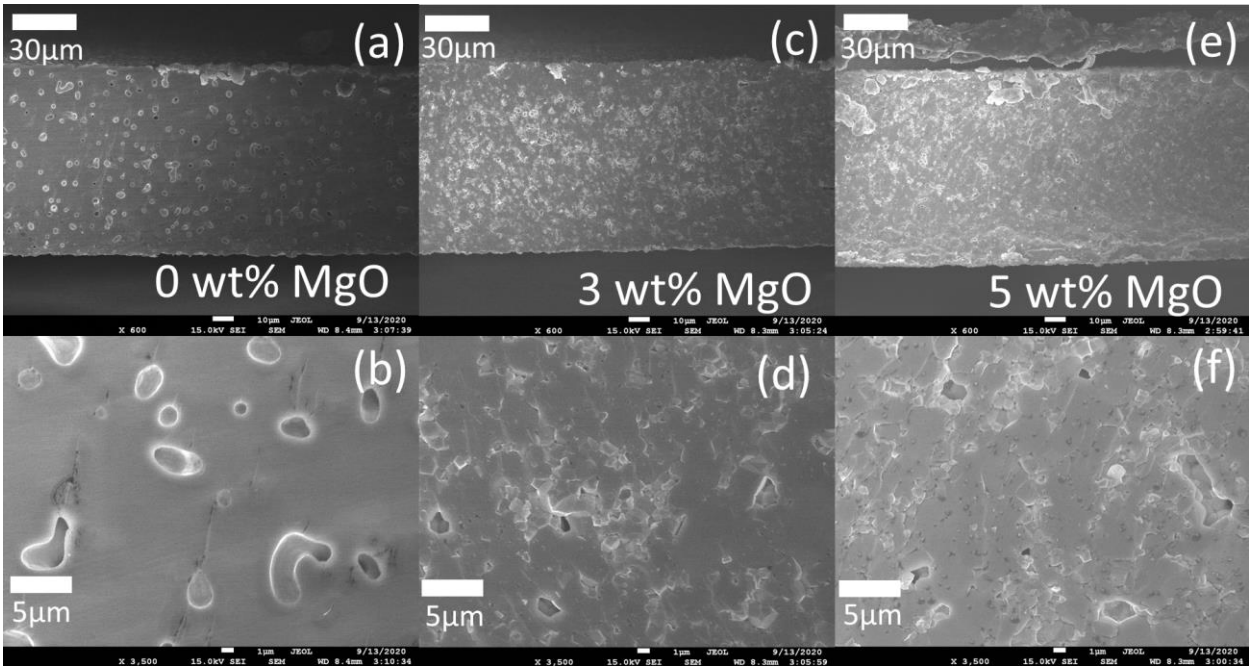

Figure 3. Microstructural impact of MgO addition to Al-LLZO sheets. SEM fracture section micrographs of Al-LLZO sheets sintered at 1115°C for 3 h containing (a, b) 0 wt%., (c, d) 3 wt%., and (e, f) 5 wt%. MgO.

Sintered Pellets

Pellet samples were produced as an attempt to clarify the detrimental effect of MgO content above 5 wt% on ionic conductivity demonstrated in the Al-LLZO sheets. Additionally, they served as demonstration of the significance of sample geometry to Li evaporation and resulting sintered Al-LLZO properties. Reduced surface area to volume ratios for pellets (14 cm^{-1} vs 150 cm^{-1} for sheets) is expected to reduce Li evaporation during sintering. Therefore, the Li_2CO_3 content was reduced from 5. to 3 wt%. for pellets and sintering times were increased to 7 h at 1115°C. These measures were insufficient to offset the reduced surface area, and all pellet samples produced contained tetragonal LLZO (Figure 4) and had ionic conductivities $<4x10^{-5}$ S/cm. Pellet densities were between 88 and 89% of theoretical over a wide range of MgO contents (0 to 7 wt%). The amount of MgO did not appear to have a significant effect on phases present, ionic conductivity, or density. The microstructural effects of the MgO were also limited by the longer sintering times and reduced Li evaporation (Figure S2). Only 7 wt% MgO pellets remained fine grained (<5µm). Course grained microstructures with grains >100µm and intragranular porosity indicative of AGG were present in pellets with up to 5 wt% MgO. This comparison of pellet and sheet properties illustrates that Li concentration, additive amounts, and sintering conditions must all be re-optimized when changing sample geometry.

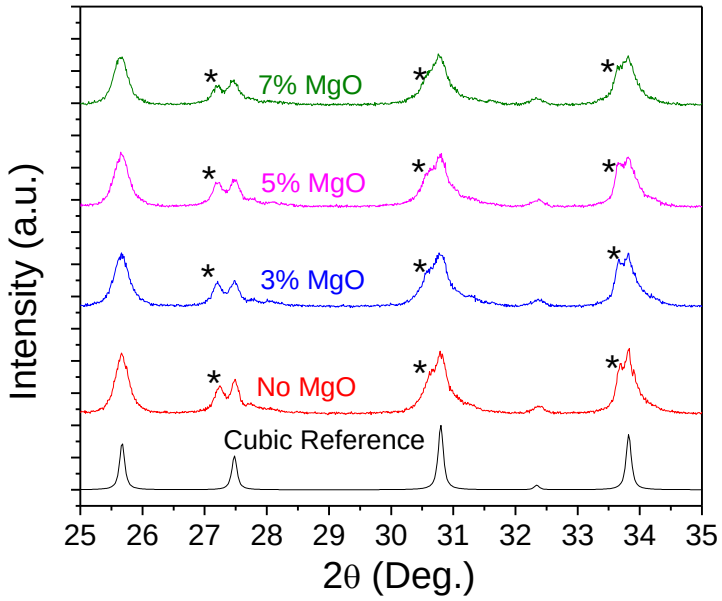

Figure 4. Decreased Li evaporation in pellets with a reduced surface area to volume ratio. Al-LLZO Pellets with 3 wt%. Li_2CO_3 sintered at 1115°C for 7 h with 0% (red), 3% (blue), 5% (pink), and 7% (green) wt. MgO. Peaks from the Li-rich tetragonal phase are identified with a *.

Tape Casting Optimization

The following section discusses the development and optimization of several tape casting systems for use with Al-LLZO and the final sintered properties of Al-LLZO sheets produced with those systems. One of the systems developed is water-based and uses methylcellulose as a binder. Aqueous tape casting systems have several health and safety advantages when compared to solvent-based systems. Volatile organic solvents require special handling to mitigate fire risks, chronic exposure for workers, and environmental release which can be avoided with aqueous systems. Aqueous systems, however, tend to be more difficult to process and optimize. The high surface energy of water can lead to tapes de-wetting from the carrier films. Water also interacts with ceramic powders more readily than most solvents, leading to dissolution and double layer effects which can have an impact on slurry dispersion [20].

Dispersant Optimization

Settling of dispersed Al-LLZO particles was used as a convenient tool to screen dispersants and optimize dispersant loadings. In a typical settling experiment with an effective dispersant, increasing dispersant loading causes a reduction in packed bed height until reaching a maximum bed density, at which point additional dispersant has no further effect [20]. For solvent-based systems DS002 behaved as expected (Figure 5). Optimal dispersion was obtained with 0.020-0.025 grams of DS002 per gram of Al-LLZO containing 3 wt%. of Li_2CO_3, and this loading was selected for further tape development. In contrast, Menhaden fish oil did not promote dispersion and settling at any concentration studied.

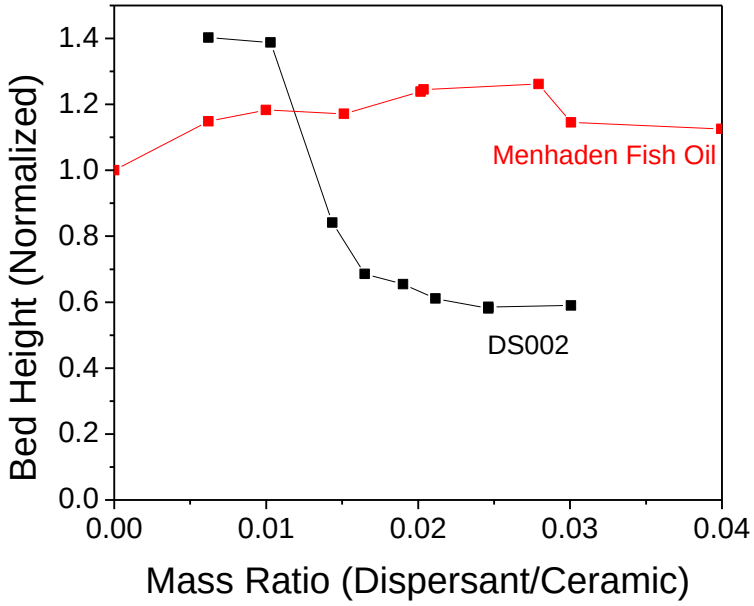

Figure 5. Dispersant behavior in toluene. Bed height of Al-LLZO with 3 wt%. Li_2CO_3 dispersed in MFO (red) and DS002 Phosphate Ester (black) after 14 days of settling.

Screening dispersants for aqueous systems was inconclusive. No tested dispersant displayed the expected settling behavior within the two-week time frame (Figure 6). In fact, a stable dispersion

was prepared with water and no additional dispersant. It may be that the Al-LLZO powder is well dispersed by electrostatic effects in aqueous environments, and the dispersion is stable indefinitely at the concentrations tested. In contrast to the other dispersants, high-molecular weight polyacrylic acid (PAA) settled to its final height immediately upon pouring into the test tube. This indicates that PAA caused undesirable agglomeration of the Al-LLZO/MgO/Li_2CO_3 slurry, allowing for very rapid settling.

Despite not having a clear impact on dispersion of Al-LLZO in water, additives were found to be critical for wetting of the slurry on the SiPET tape casting substrate. Wetting behavior of aqueous methylcellulose tapes with various additives is shown in Figure 6. Slurries containing both Dispex Ultra PA 4560 and Dynol 604 wet the substrate well while either additive alone is ineffective. When only the Dispex dispersant is present, the tape film breaks up into droplets. When only Dynol 604 wetting agent is used, the tape slurry recedes from the edge and pools in a thick line. The combination of Dispex and Triton X-100 prevented complete de-wetting but the tapes receded substantially at the edges and had poor yield of usable tape area. It should be noted that uncoated PET was investigated for use as a carrier film to avoid de-wetting. Aqueous tapes wet the PET well, however, they bonded too strongly to the carrier and could not be removed intact.

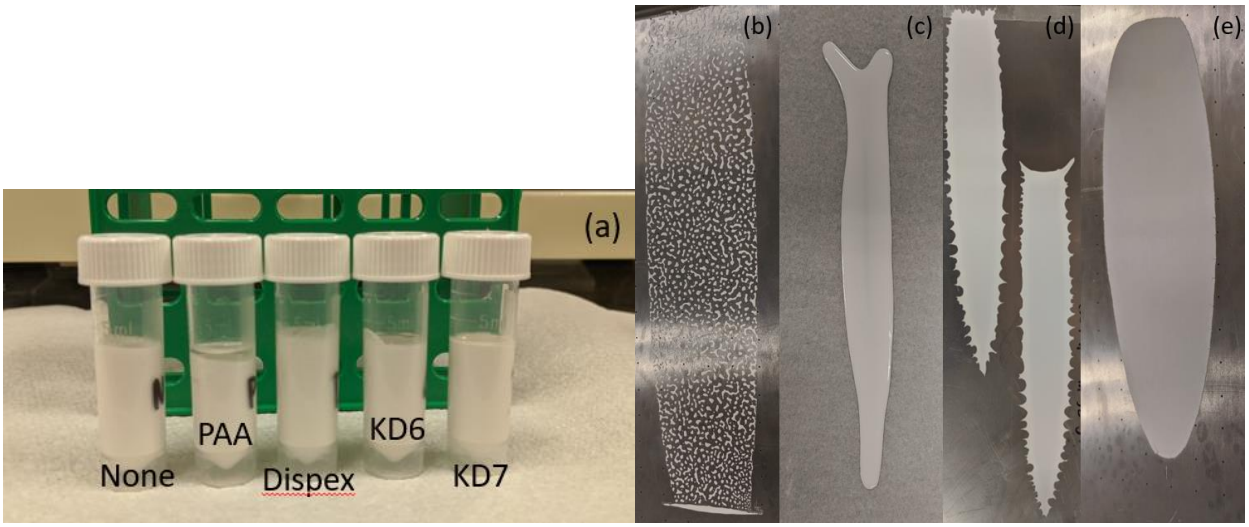

Figure 6. (a) Aqueous dispersant screening of Al-LLZO slurries containing 1.1 wt% dispersant: (left to right) no dispersant, high-molecular weight poly(acrylic acid) (PAA), Dispex Ultra PA 4560, Hypermer KD-6, and Hypermer KD-7. (b-e) The effect of additives on methylcellulose-based aqueous slurry wetting behavior. Photographs of tapes cast on SiPET with the additives (b) Dispex Ultra PA 4560, (c) Dynol 604, (d) Dispex with Triton X-100, and (e) Dispex with Dynol 604.

Green density and tape properties

A wide range of aqueous and non-aqueous solvent/binder systems were selected for comparison, based on the literature (Table 1) and consultation with tape casting materials vendors. In order to compare the tape casting systems directly, Al-LLZO with 5 wt% Li_2CO_3 and 5 wt% MgO was chosen as a standard ceramic composition because it demonstrated the highest density after sintering optimization. The selected tape casting binder/solvent systems are compared in Table 5 with assessment of several important processing characteristics. The water-based WB4101 and PVA systems gel immediately upon contact with Al-LLZO rendering them unusable. These were removed from further consideration. A viable aqueous system was identified, using methyl-cellulose binder. The largest challenge in producing methylcellulose tapes is the prevention of de-wetting while maintaining easy release of the tape from the carrier film substrate, as discussed

above. All of the solvent-based systems present some level of health and safety concern because of their volatile organic solvents. In addition, the PVB binder requires hazardous phthalate-based plasticizers. Both PVB and ethylcellulose systems produce very brittle tapes that can be difficult to handle. The MSB1-13 system is the easiest to use and produces the most flexible and strong green tapes.

Table 5. Summary of tape casting system usability

Binder System	Solvent Health/ Safety	LLZO Compatibility	Slurry Foaming	Ease of Carrier Release	Green Mechanical Properties	Oxide-Only Density of Laminates (%)
PVA	Aqueous	Gels				
PII – WB4101	Aqueous	Gels	-	-	-	-
Methyl-Cellulose	Aqueous	Yes	Yes, Controllable	Controllable De-wetting	Good	40.2
PVB	Ethanol/ Acetone	Yes	No	Poor	Brittle	44.3
Ethyl-cellulose	Toluene/ Ethanol	Yes	Minor	Good	Brittle	43.9
PII - MSB1-13	Toluene/ Xylene	Yes	No	Good	Very Good	41.7

Red cells indicate disqualifying issues, yellow cells indicate drawbacks or challenges that do not prevent the system from being usable, green cells indicate desirable properties.

Subsequent to screening, the slurries were compared in more detail. Table S1 lists the compositions of the tape casting slurries. Low-binder versions of the methylcellulose and MSB1-3 slurries were produced to determine if there was a tradeoff between green properties and final properties, e.g. if lower binder content produces weaker tape but higher sintered density. Table 6 compares the green and sintered properties of the tapes. The mechanical integrity was characterized using a bend test around rods of various diameters. Both the methylcellulose and MSB1-13 systems demonstrated much greater flexibility and strength than either ethylcellulose or

PVB. Methylcellulose tapes would break around 2 or 3 mm diameter rods while MSB1-13 tapes showed exceptional mechanical properties and could be folded in half without cracking. Ethylcellulose tapes were much less flexible and cracked around rods less than 10 mm in diameter. PBV tapes could not bend around the largest 14 mm diameter rod. Photos of flexible freestanding tapes prepared with the methylcellulose and MSB1-13 systems are shown in Figure 7.

Table 6. Comparison of green and sintered properties of tape cast Al-LLZO sheets

Binder System	Slurry Ceramic %wt.	Ceramic Solids %wt.	Single Layer Oxide Only % Density	Laminate Oxide Only % Density	Bend test Diameter (mm)	Comment	3hr 1115°C Sintered % Density	Sintered Conductivity (S/cm x10^{-4})
Methyl-cellulose	38.6	88.4	30.3±0.3	40.2±0.5	2-3	Good	91.0±0.8	2.3±0.4
Methyl-cellulose Low Binder	38.7	89.2	30.4±0.3	44±1	3	De-wetting	91.8±0.6	2.3±0.4
Ethyl-cellulose	40.1	88.7	32.2±0.6	43.9±0.3	10	Mud Cracks	89.6±0.8	2.3±0.9
PVB	41.7	84.7	35±3	44.3±0.8	>14	Brittle	92.3±0.3	2.25±0.5
MSB1-13	37.9	89.4	38 ±1	41.3±0.2	<2	Excellent, can be folded	87.9±0.7	1.7±0.9
MSB1-13 Low Binder	45.6	93.9	35.6±0.4	42±2	3	Difficult carrier release	88.0±0.6	1.6±0.8

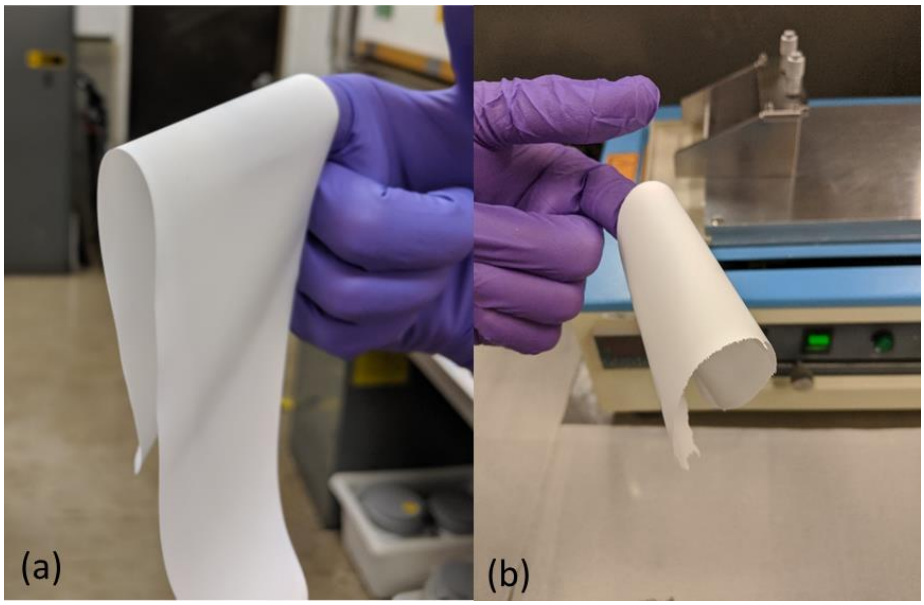

Figure 7. Photographs of green Al-LLZO tapes using (a) MSB1-13 and (b) methylcellulose binders.

In general, as tapes progressed through the processing to the final sintered Al-LLZO sheet the differences between the binder systems were reduced. As part of this processing, tapes were laminated into stacks of 4 layers in order to produce thicker ceramic sheets which were more easily handled for analysis and would be more representative of the thicker bi/ trilayer structures used for assembling solid state batteries[22-24, 26, 28]. The as-cast oxide-only density of the tapes ranged widely from 30.3 % (methylcellulose) to 38.0% (MSB1-13) but the range for laminates was narrower, 40.2 to 44.6%. This narrower range for laminates is intuitive because the green tapes have similar ceramic-to-additive ratios but appear to have different residual porosities. The lamination process eliminates most of the residual porosity from the green tapes.

The final sintered density also appears to be weakly coupled to the green density of the laminates. For example, the low binder methylcellulose laminates were 4.4 percentage points more dense than the standard methylcellulose laminates but after sintering the difference is only 0.7 percentage points. The final sintered density for both compositions of MSB1-13 tapes is notably less than the

others at approximately 88%. We speculate that the enhanced density of the methylcellulose, ethylcellulose, and PVB binder systems is due to water content in the solvents of those systems. In water, LLZO is known to protonate by exchanging Li^+ for H^+ ions and the Li+ can then further react with CO_2 to produce Li_2CO_3 [16, 27]. During sintering, the Li_2CO_3 decomposes and the Li is returned to the LLZO lattice [27, 33]. This reaction or the additional transient Li_2CO_3 liquid phase produced by this reaction could explain the discrepancy in densification between the aqueous methylcellulose and solvent-based MSB1-13 systems[14]. In the cases of ethylcellulose and PVB it is possible that the ethanol and/or acetone could contain some amount of water contamination and produce a similar effect.

Conclusions

Optimization of sintering time and MgO content in Al-LLZO sheets identified a tradeoff between ionic conductivity and density. Al-LLZO sheets with 3% MgO were ~88% dense with $>4x10^{-4}$ S/cm conductivity while sheets with 5 wt%. MgO were ~91% dense with conductivity between 2 and $3x10^{-4}$ S/cm. Through a comparison of the phase stability of tape cast sheets and pelletized samples the importance of Li content optimization on an Al-LLZO part's final properties was also demonstrated. While these sheet properties do not represent the highest densities or conductivities seen in the literature the focus of this work was to optimize the ceramic composition and sintering conditions sufficiently to enable a comparison of tape casting binder systems. Future work may see improved sheet properties though alternative ceramic compositions (e.g. Ga, Ta or Nb doped LLZO) or powder morphology (e.g. finer particles, bimodal particle size distribution, or surface treatments).

A wide variety of tape casting systems were assessed for use with Al-LLZO. Both aqueous and solvent-based binder systems were capable of producing high density sintered Al-LLZO, after careful optimization of additives and slurry recipes. In contrast to previous efforts, a direct comparison of the tape casting systems was achieved by using the same Al-LLZO powder and processing methods for all candidates. The tape casting binder/solvent systems studied here produce a wide range of tape usability, as-cast density, and mechanical properties. As long as the system is well optimized, however, binder choice alone does not have a large effect on the properties of the final sintered Al-LLZO. Thus, green tape properties should not be used as a proxy for quality of the final sintered part, but they may be very important to manufacturability considerations such as uniformity, defect concentration, lamination processing, and handling strength. Of the tested binders, methylcellulose can be recommended for being environmentally friendly and presenting fewer health and safety issues while the MSB1-13 binder can be recommended for superior green mechanical properties.

ASSOCIATED CONTENT

Supporting Information

Tape casting slurry compositions; Dilatometry of Al-LLZO pellets with 0 wt% and 5 wt% MgO; Viscosity of methylcellulose, ethylcellulose and MSB1-13 slurries; SEM images of sintered Al-LLZO pellets with 0 wt%, 3 wt% and 7 wt% MgO

AUTHOR INFORMATION

Corresponding Author

Michael C. Tucker − Lawrence Berkeley National Laboratory, Berkeley, California;

orcid.org/0000-0002-8508-499X; E-mail: mctucker@lbl.gov

Other Authors

Robert A. Jonson − Lawrence Berkeley National Laboratory, Berkeley, California; orcid.org/0000-0001-9314-4609

Eongyu Yi − Lawrence Berkeley National Laboratory, Berkeley, California; orcid.org/0000-0002-6079- 9382

Fengyu Shen − Lawrence Berkeley National Laboratory, Berkeley, California; orcid.org/0000-0003-3818-176X

Notes

The authors declare no competing financial interest.

ACKNOWLEDGMENTS

This work was supported by the Vehicle Technologies Office, Office of Energy Efficiency and Renewable Energy, of the U.S. Department of Energy. The authors thank Peter Faguy, Mark Wesselmann, and Kostadin Petkov for helpful discussion. This work was funded in part by the U.S. Department of Energy under contract no. DE-AC02-05CH11231. The views and opinions of the authors expressed herein do not necessarily state or reflect those of the United States Government or any agency thereof. Neither the United States Government nor any agency thereof, nor any of their employees, makes any warranty, expressed or implied, or assumes any legal liability or responsibility for the accuracy, completeness, or usefulness of any information, apparatus, product, or process disclosed, or represents that its use would not infringe privately owned rights.

REFERENCES

1. Ramakumar, S.;C. Deviannapoorani;L. Dhivya;L.S. Shankar; and R. Murugan, *Lithium garnets: Synthesis, structure, Li + conductivity, Li + dynamics and applications.* Progress in Materials Science, 2017. **88**: p. 325-411.
2. Wang, C.;K. Fu;S.P. Kammampata;D.W. McOwen;A.J. Samson;L. Zhang;G.T. Hitz;A.M. Nolan;E.D. Wachsman;Y. Mo;V. Thangadurai; and L. Hu, *Garnet-Type Solid-State Electrolytes: Materials, Interfaces, and Batteries.* Chem Rev, 2020. **120**(10): p. 4257-4300.
3. Wolfenstine, J.;J.L. Allen;J. Read; and J. Sakamoto, *Chemical stability of cubic Li7La3Zr2O12 with molten lithium at elevated temperature.* Journal of Materials Science, 2013. **48**(17): p. 5846-5851.
4. Miara, L.J.;W.D. Richards;Y.E. Wang; and G. Ceder, *First-Principles Studies on Cation Dopants and Electrolyte|Cathode Interphases for Lithium Garnets.* Chemistry of Materials, 2015. **27**(11): p. 4040-4047.
5. Thompson, T.;S. Yu;L. Williams;R.D. Schmidt;R. Garcia-Mendez;J. Wolfenstine;J.L. Allen;E. Kioupakis;D.J. Siegel; and J. Sakamoto, *Electrochemical Window of the Li-Ion Solid Electrolyte Li7La3Zr2O12.* ACS Energy Letters, 2017. **2**(2): p. 462-468.
6. Awaka, J.;N. Kijima;H. Hayakawa; and J. Akimoto, *Synthesis and structure analysis of tetragonal Li7La3Zr2O12 with the garnet-related type structure.* Journal of Solid State Chemistry, 2009. **182**(8): p. 2046-2052.
7. Samson, A.J.;K. Hofstetter;S. Bag; and V. Thangadurai, *A bird's-eye view of Li-stuffed garnet-type Li7La3Zr2O12 ceramic electrolytes for advanced all-solid-state Li batteries.* Energy & Environmental Science, 2019. **12**(10): p. 2957-2975.
8. Liu, Q.;Z. Geng;C. Han;Y. Fu;S. Li;Y.-b. He;F. Kang; and B. Li, *Challenges and perspectives of garnet solid electrolytes for all solid-state lithium batteries.* Journal of Power Sources, 2018. **389**: p. 120-134.
9. Shin, D.O.;K. Oh;K.M. Kim;K.Y. Park;B. Lee;Y.G. Lee; and K. Kang, *Synergistic multi-doping effects on the Li7La3Zr2O12 solid electrolyte for fast lithium ion conduction.* Sci Rep, 2015. **5**: p. 18053.
10. Meier, K.;T. Laino; and A. Curioni, *Solid-State Electrolytes: Revealing the Mechanisms of Li-Ion Conduction in Tetragonal and Cubic LLZO by First-Principles Calculations.* The Journal of Physical Chemistry C, 2014. **118**(13): p. 6668-6679.
11. Murugan, R.;V. Thangadurai; and W. Weppner, *Fast lithium ion conduction in garnet-type Li(7)La(3)Zr(2)O(12).* Angew Chem Int Ed Engl, 2007. **46**(41): p. 7778-81.
12. Liu, K.;J.-T. Ma; and C.-A. Wang, *Excess lithium salt functions more than compensating for lithium loss when synthesizing Li6.5La3Ta0.5Zr1.5O12 in alumina crucible.* Journal of Power Sources, 2014. **260**: p. 109-114.
13. Yi, E.;W. Wang;J. Kieffer; and R.M. Laine, *Flame made nanoparticles permit processing of dense, flexible, Li+ conducting ceramic electrolyte thin films of cubic-Li7La3Zr2O12 (c-LLZO).* Journal of Materials Chemistry A, 2016. **4**(33): p. 12947-12954.
14. Yi, E.;W. Wang;J. Kieffer; and R.M. Laine, *Key parameters governing the densification of cubic-Li7La3Zr2O12 Li+ conductors.* Journal of Power Sources, 2017. **352**: p. 156-164.
15. Xiang, X.;F. Chen;Q. Shen;L. Zhang; and C. Chen, *Effect of the lithium ion concentration on the lithium ion conductivity of Ga-doped LLZO.* Materials Research Express, 2019. **6**(8).

16. Jin, Y. and P.J. McGinn, *Al-doped Li7La3Zr2O12 synthesized by a polymerized complex method.* Journal of Power Sources, 2011. **196**(20): p. 8683-8687.
17. Huang, X.;T. Xiu;M.E. Badding; and Z. Wen, *Two-step sintering strategy to prepare dense Li-Garnet electrolyte ceramics with high Li+ conductivity.* Ceramics International, 2018. **44**(5): p. 5660-5667.
18. Huang, X.;Y. Lu;Z. Song;T. Xiu;M.E. Badding; and Z. Wen, *Preparation of dense Ta-LLZO/MgO composite Li-ion solid electrolyte: Sintering, microstructure, performance and the role of MgO.* Journal of Energy Chemistry, 2019. **39**: p. 8-16.
19. Huang, X.;C. Liu;Y. Lu;T. Xiu;J. Jin;M.E. Badding; and Z. Wen, *A Li-Garnet composite ceramic electrolyte and its solid-state Li-S battery.* Journal of Power Sources, 2018. **382**: p. 190-197.
20. Mistler, R.E. and E.R. Twiname, *Tape casting: theory and practice*. 2000: American ceramic society. p.2-6, 28-29, 225-228.
21. Hanc, E.;W. Zając;L. Lu;B. Yan;M. Kotobuki;M. Ziąbka; and J. Molenda, *On fabrication procedures of Li-ion conducting garnets.* Journal of Solid State Chemistry, 2017. **248**: p. 51-60.
22. Fu, K.;Y. Gong;G.T. Hitz;D.W. McOwen;Y. Li;S. Xu;Y. Wen;L. Zhang;C. Wang;G. Pastel;J. Dai;B. Liu;H. Xie;Y. Yao;E.D. Wachsman; and L. Hu, *Three-dimensional bilayer garnet solid electrolyte based high energy density lithium metal–sulfur batteries.* Energy & Environmental Science, 2017. **10**(7): p. 1568-1575.
23. Hitz, G.T.;D.W. McOwen;L. Zhang;Z. Ma;Z. Fu;Y. Wen;Y. Gong;J. Dai;T.R. Hamann;L. Hu; and E.D. Wachsman, *High-rate lithium cycling in a scalable trilayer Li-garnet-electrolyte architecture.* Materials Today, 2019. **22**: p. 50-57.
24. Hamann, T.;L. Zhang;Y. Gong;G. Godbey;J. Gritton;D. McOwen;G. Hitz; and E. Wachsman, *The Effects of Constriction Factor and Geometric Tortuosity on Li-Ion Transport in Porous Solid-State Li-Ion Electrolytes.* Advanced Functional Materials, 2020. **30**(14).
25. Chen, F.;S. Cao;X. Xiang;D. Yang;W. Zha;J. Li;Q. Shen; and L. Zhang, *The Tape-Casting And Pas Sintering Of Llzo Ceramic Membrane Electrolyte*, in *Proceeding of the 42nd International Conference on Advanced Ceramics and Composites*. 2019. p. 221-230.
26. Yi, E.;H. Shen;S. Heywood;J. Alvarado;D.Y. Parkinson;G. Chen;S.W. Sofie; and M.M. Doeff, *All-Solid-State Batteries Using Rationally Designed Garnet Electrolyte Frameworks.* ACS Applied Energy Materials, 2020. **3**(1): p. 170-175.
27. Ye, R.J.;C.L. Tsai;M. Ihrig;S. Sevinc;M. Rosen;E. Dashjav;Y.J. Sohn;E. Figgemeier; and M. Finsterbusch, *Water-based fabrication of garnet-based solid electrolyte separators for solid-state lithium batteries.* Green Chemistry, 2020. **22**(15): p. 4952-4961.
28. Shen, H.;E. Yi;S. Heywood;D.Y. Parkinson;G. Chen;N. Tamura;S. Sofie;K. Chen; and M.M. Doeff, *Scalable Freeze-Tape-Casting Fabrication and Pore Structure Analysis of 3D LLZO Solid-State Electrolytes.* ACS Appl Mater Interfaces, 2020. **12**(3): p. 3494-3501.
29. Gao, K.;M. He;Y. Li;Y. Zhang;J. Gao;X. Li;Z. Cui;Z. Zhan; and T. Zhang, *Preparation of high-density garnet thin sheet electrolytes for all-solid-state Li-Metal batteries by tape-casting technique.* Journal of Alloys and Compounds, 2019. **791**: p. 923-928.

30. Jonson, R.A. and P.J. McGinn, *Tape casting and sintering of Li7La3Zr1.75Nb0.25Al0.1O12 with Li3BO3 additions.* Solid State Ionics, 2018. **323**: p. 49-55.
31. Liu, K. and C.-A. Wang, *Honeycomb-alumina supported garnet membrane: Composite electrolyte with low resistance and high strength for lithium metal batteries.* Journal of Power Sources, 2015. **281**: p. 399-403.
32. Cheng, L.;E.J. Crumlin;W. Chen;R. Qiao;H. Hou;S. Franz Lux;V. Zorba;R. Russo;R. Kostecki;Z. Liu;K. Persson;W. Yang;J. Cabana;T. Richardson;G. Chen; and M. Doeff, *The origin of high electrolyte-electrode interfacial resistances in lithium cells containing garnet type solid electrolytes.* Phys Chem Chem Phys, 2014. **16**(34): p. 18294-300.
33. Cheng, L.;M. Liu;A. Mehta;H. Xin;F. Lin;K. Persson;G. Chen;E.J. Crumlin; and M. Doeff, *Garnet Electrolyte Surface Degradation and Recovery.* ACS Applied Energy Materials, 2018. **1**(12): p. 7244-7252.